Astron. Astrophys. 359, 148–158 (2000)

ASTRONOMY AND ASTROPHYSICS

The ISO spectroscopic view of the HH 24–26 region⋆

M. Benedettini[1], T. Giannini[1,2,3], B. Nisini[2], E. Tommasi[4], D. Lorenzetti[2], A.M. Di Giorgio[1], P. Saraceno[1], H.A. Smith[5], and G.J. White[6,7]

[1] CNR-Istituto di Fisica dello Spazio Interplanetario, Area di Ricerca di Tor Vergata, via del Fosso del Cavaliere 100, 00133 Roma, Italy
[2] Osservatorio Astronomico di Roma, via Frascati 33, 00040 Monte Porzio, Italy
[3] Università La Sapienza, via Lancisi 29, 00161 Roma, Italy
[4] Agenzia Spaziale Italiana, via di Villa Patrizi 13, 00161 Roma, Italy
[5] Harvard - Smithsonian Center for Astrophysics, 60 Garden Street, Cambridge, MA, USA
[6] Queen Mary and Westfield College, University of London, Mile End Road, London E1 4NS, UK
[7] Stockholm Observatory, 133 36 Saltsjobaden, Sweden

Received 29 September 1999 / Accepted 22 April 2000

Abstract. We report the results of an investigation, performed with the ISO spectrometers (LWS and SWS), on the star forming region associated with the Herbig-Haro objects HH 24–25 and 26. Low-resolution LWS spectra (45-197 μm) were observed towards the HH24MMS, HH25MMS and HH26IR sources as well as the HH26IR outflow. In addition, SWS scans of the pure H_2 rotational lines towards HH24MMS were acquired. Emission from [O I] 63 μm and [C II] 158 μm appears widespread while molecular transitions of carbon monoxide and water vapour were detected only towards HH25MMS and the blue lobe of HH26IR. From the analysis of the observed emission we deduce that the gas towards HH24MMS and HH25MMS is excited at densities $\sim 10^6$ cm^{-3} and temperatures ranging from 650 to 1400 K in HH24MMS and from 150 to 550 K in HH25MMS. Along the blue lobe of the HH26IR outflow, a more diffuse ($n_{\rm H_2} \sim 10^4$ cm^{-3}) and warm ($T \sim 1800$ K) gas is found. Both the molecular (CO, H_2O and H_2) and atomic ([O I]) emission in the three sources can be interpreted as due to shock excitation, and a mixture of both *C*- and *J*-type shocks are required to reproduce most of the observed characteristics of the spectra. The derived water abundances ($3\,10^{-7}$-$9\,10^{-6}$) are lower than expected in warm shock excited gas, a result which has also been found in other similar regions investigated with ISO. The total cooling derived from the gas component traced by the FIR lines is always of the same order or larger than the cooling due to the molecular hydrogen as traced by the H_2 2.12 μm line; although this latter could be underestimated if the dust extinction is not negligible, however it is evident that a significant fraction of the energy released in the shocks is re-radiated away by the far infrared lines. Finally, the [C II]158μm line intensities are rather constant at all of the observed positions, excluding the presence of strong photo-dissociation regions related to the nearby IR sources.

Send offprint requests to: M. Benedettini (milena@ifsi.rm.cnr.it)

⋆ Based on observations with ISO, an ESA project with instruments funded by ESA Member States and with the participation of ISAS and NASA

Key words: stars: formation – stars: individual: HH24MMS, HH25MMS, HH26IR – ISM: jets and outflows – infrared: ISM: lines and bands

1. Introduction

The HH 24-25-26 region is located in the L1630 Orion dark cloud at distance of ∼400 pc (Anthony-Twarog 1982) and presents a quite complex morphology due to strong star formation activity. The region is rich in young stellar objects including the two very young and embedded protostars (Class 0, Andre et al. 2000) HH24MMS (Chini et al. 1993) and HH25MMS (Bontemps et al. 1995), the Class I protostar HH26IR (Davis et al. 1997) and four more evolved IRAS sources, i.e. SSV59, SSV60, SSV61 and SSV63 (Strom et al. 1976), whose luminosities range between 15 and 25 $L_\odot$. Compact jets, traced by means of both the 2.12 μm H_2 line and CO mm observations (Gibb & Davis 1998; Bontemps et al. 1996), emanate from HH24MMS and HH25MMS, while HH26IR drives a more extended molecular outflow (Gibb & Heaton 1993). Observations in the 2.12 μm H_2 rovibrational line (Davis et al. 1997) reveal a string of shocked H_2 knots along the axis of the HH25MMS and HH26IR outflows. Herbig-Haro objects (HH24, HH25 and HH26) are associated with each of these three sources. Radio maps of the region (Gibb & Heaton 1993) reveal a string of dense molecular cores, extending north-south for about 6′, some of which are associated with the infrared sources.

In this paper we report the results of a spectroscopic investigation of the region with the Infrared Space Observatory (ISO, Kessler et al. 1996). The far infrared spectral band covered by the ISO spectrometers extends from 3 to 200 μm and includes transitions from atoms (e.g. O^o and C^+) and molecules (e.g. CO, H_2O, H_2 and OH) which are expected to be copiously emitted in the excitation conditions prevailing in star forming regions. Such emission lines have the advantage of being less sensitive to the extinction which can be severe for deeply embedded objects

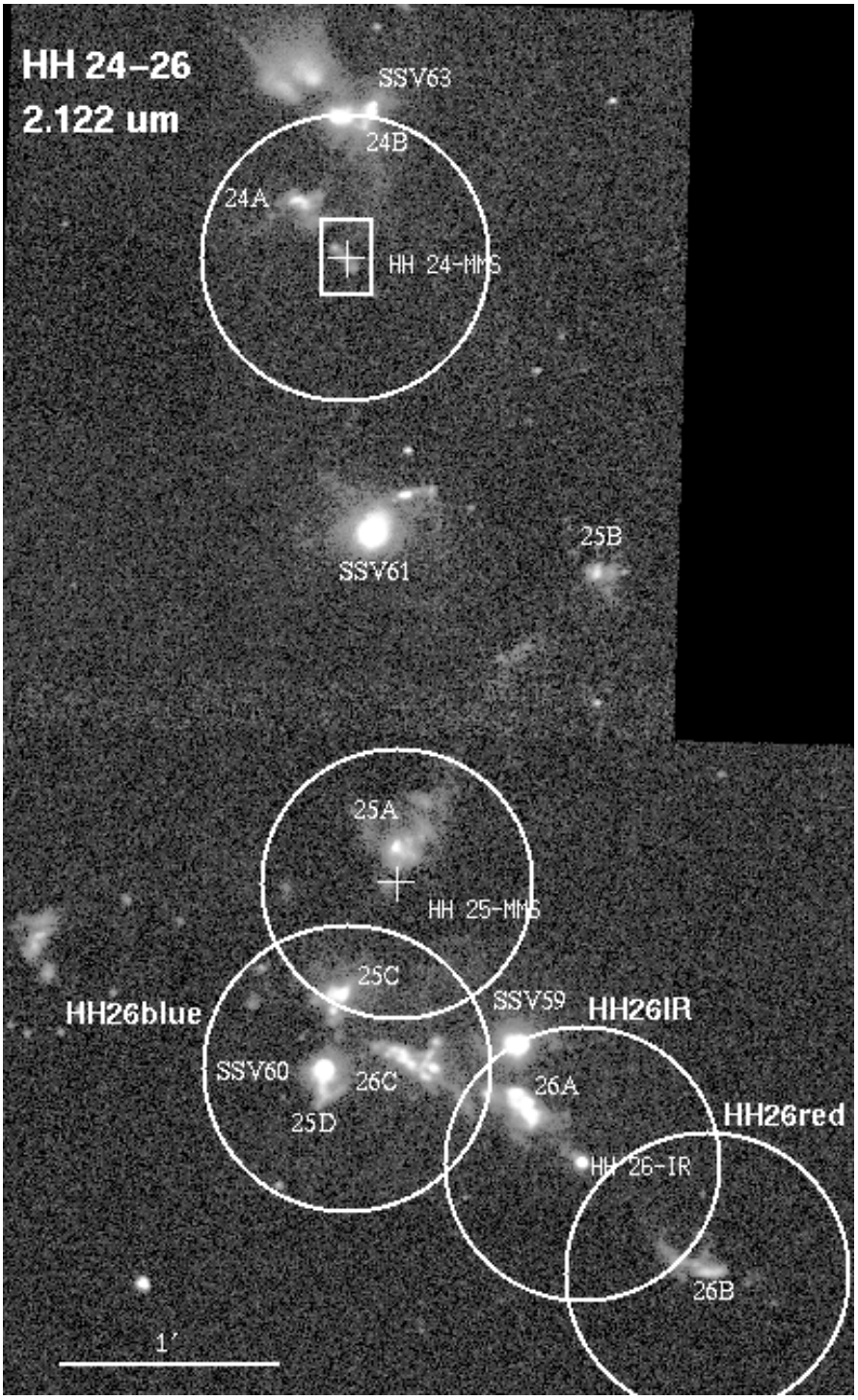

Fig. 1. Narrow-band image of the HH24–26 region at 2.122 μm (H_2+continuum) from Davis et al. (1997) with superimposed the LWS (circle) and SWS (rectangle) beams on the targetted positions. The crosses mark the positions of HH24MMS and HH25MMS. The blue and the red lobe of the HH26IR flow are associated with 26A, C and 26B respectively.

like the Class 0 sources HH24MMS and HH25MMS, making observations of the warm circumstellar environment difficult in the near infrared. Therefore the analysis of far infrared lines provides a powerful diagnostic tool of the physical conditions and energy budget in complex star forming regions like HH24–26.

In Sect. 2 of this paper we will describe the observations and the reduction methods. In Sect. 3 we will present the main observational results, together with the model fits on the molecular lines using a Large Velocity Gradient code. In Sect. 4 the SEDs of the three protostars will be presented. Finally, in Sect. 5 the excitation mechanisms will be discussed for the different parts of the investigated region and in Sect. 6 some global conclusions will be given.

2. Observations and data reduction

Full grating scans (i.e. from 45 to 197 μm with $\lambda/\Delta\lambda \sim 200$) centered on HH24MMS, HH25MMS and HH26IR, as well as along the HH26IR outflow were obtained with the Long Wave-

Table 1. Journal of the observations.

Source	Date	# orbit	α(2000)			δ(2000)			t_{int}	n_s
			h	m	s	°	′	″	sec	
HH24MMS SWS	14 Oct 97	698	5	46	08.6	-0	10	40.8	-	-
HH24MMS	14 Oct 97	698	5	46	08.6	-0	10	40.8	10	25
HH25MMS	10 Oct 97	694	5	46	06.7	-0	13	24.7	10	25
HH26blue	10 Oct 97	694	5	46	08.9	-0	14	26.8	4.8	12
HH26IR	10 Oct 97	694	5	46	03.9	-0	14	52.5	4.8	12
HH26red	10 Oct 97	694	5	46	01.6	-0	15	23.3	4.8	12

Notes: t_{int}=integration time per spectral sample; n_s = number of spectral scans

length Spectrometer (LWS, Clegg et al. 1996) on board ISO. The journal of the observations is presented in Table 1 and the target positions are shown in Fig. 1, where the LWS and SWS fields of view are superimposed on the 2.12 μm image taken from Davis et al. (1997). With the relatively large LWS beam of $\sim$80″ we were able to cover the HH26IR outflow with three partially overlapping observations, centered on the IR source and on the blue and the red outflow lobes (called HH26IR, HH26blue and HH26red respectively). For HH24MMS and HH25MMS, a single LWS measurement encompasses the MM source as well as the associated HH and jet.

The LWS measurements were obtained by oversampling the spectra by a factor 4. Each spectral sample was repeated a number of times as indicated in Column 7 of Table 1 and integrated for a total time given in Column 6. The raw data were reduced using the Off-Line Processing (OLP) version 7 software and calibrated with Uranus, giving an absolute flux calibration uncertainty better than 30% (Swinyard et al. 1996). Additional reduction steps were carried out to remove spurious signal due to cosmic ray impact, to average together the scans of each detector and to remove the interference fringes which affect the LWS spectra.

HH24MMS was also observed using the Short Wavelength Spectrometer (SWS, de Graauw et al. 1996) in the AOT02 grating mode, to scan the H_2 (ν= 0→0) rotational lines from (0-0)S(1) to (0-0)S(5) obtaining line spectra covering a wavelength range 0.1 μm wide, at 6.9, 8.0 and 9.7 μm and 0.2 μm at 12.3 and 17 μm. The resolution was $\lambda/\Delta\lambda \sim 1200$ and the aperture size was 14″× 27″ for the (0-0)S(1) and S(2) lines and 14″× 20″ for the (0-0)S(3), S(4) and S(5) lines. Also all the other positions listed in Table 1 were scheduled to be observed with SWS but the observations were not performed because of the end of the satellite operations. The integration time for the SWS observations was 200 sec for each line. The OLP version 6 was used to process the raw data, achieving flux calibration uncertanties of about 30% (Schaeidt et al. 1996). The final spectra were obtained after de-glitching, averaging and rebinning the data to double the instrumental resolution.

3. Results and analysis

Table 2 lists the lines identified in the different spectra (Column 2) and their integrated fluxes estimated from gaussian fits to the (unresolved) line profile (Column 4) together with the 1σ error

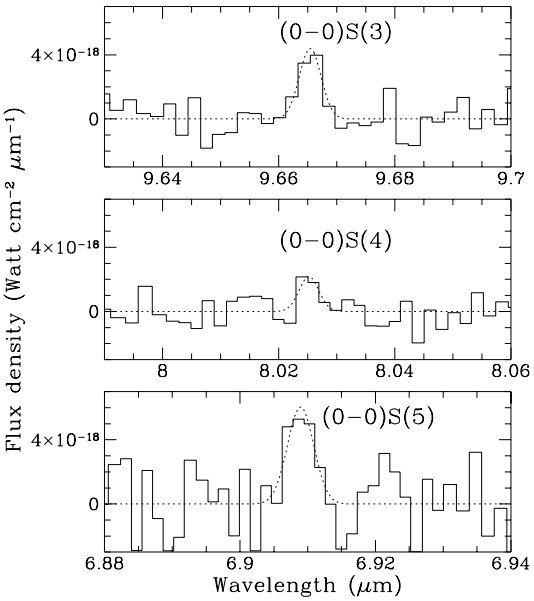

Fig. 2. Gaussian fits to the H_2 rotational lines (0-0)S(3), (0-0)S(4) and (0-0)S(5) observed in HH24MMS.

associated to the rms noise of the local baseline (Column 5). In this table we also report the vacuum wavelengths of the identified transitions (λ_{vac}, Column 1) and the observed wavelengths (λ_{obs}, Column 3). The line identification was based on the following criteria: *i)* signal to noise ratio S/N$\geq$ 3, *ii)* consistency of the FWHM with the instrumental resolution and *iii)* difference between the fitted line center and the expected wavelength less than half of the resolution element (*i.e.* 0.003 μm for $6 < \lambda < 12$ μm and 0.005 μm for $12 < \lambda < 19$ μm (SWS); 0.15 μm for $45 < \lambda < 90$ μm and 0.3 μm for $90 < \lambda < 190$ μm (LWS)).

Towards HH24MMS, out of the five H_2 (0-0) transitions scanned with SWS, only the S(3), S(4) and S(5) lines have been detected with S/N$\geq$3 (Fig. 2).

All the LWS spectra show the [O I]63 μm (Fig. 3) and the [C II]158 μm atomic lines; emission from molecular lines is however less widespread. HH25MMS has the richest molecular lines spectrum in which CO transitions from J_{up}=14 to J_{up}=18 as well as the three o-H_2O backbone lines at 179.5, 174.6 and 113.5 μm are seen. Conversely, towards HH24MMS the CO 17-16 line was the only molecular line detected. Among the three pointings covering the HH26 flow, HH26blue shows the

Table 2. Observed emission lines. Flux upper limits are 3σ.

$\lambda_{\rm vac}$ (μm)	Transition	$\lambda_{\rm obs}$ (μm)	Flux (10^{-20} W cm^{-2})	ΔFlux
HH24MMS				
6.909	H_2(0-0)S(5)	6.909	3	1
8.025	H_2(0-0)S(4)	8.026	1.1	0.4
9.665	H_2(0-0)S(3)	9.666	2.0	0.4
12.279	H_2(0-0)S(2)		$<$3	
17.035	H_2(0-0)S(1)		$<$1.2	
63.18	[O I]$^3P_1 - ^3P_2$	63.19	55	3
144.78	CO 18-17		$<$3	
145.53	[O I]$^3P_0 - ^3P_1$		$<$3	
157.74	[CII]$^3P_{3/2} - ^3P_{1/2}$	157.78	40	1
153.27	CO 17-16	153.60†	3.6	0.7
162.81	CO 16-15		$<$3	
HH25MMS				
63.18	[O I]$^3P_1 - ^3P_2$	63.21	49	2
113.54	o-H_2O 4_{14}-3_{03}	113.89†	5	1
137.20	CO 19-18		$<$4.5	
144.78	CO 18-17	144.93	6.4	0.9
145.53	[O I]$^3P_0 - ^3P_1$		$<$3	
153.27	CO 17-16	153.36	7.2	0.7
157.74	[C II]$^3P_{3/2} - ^3P_{1/2}$	157.75	29.6	0.9
162.81	CO 16-15	162.87	7.0	0.8
173.63	CO 15-14	173.62	6	1
174.63	o-H_2O 3_{03}-2_{12}	174.69	4	1
179.53	o-H_2O 2_{12}-1_{01}	179.63	10	2
186.00	CO 14-13	185.93	6	2
HH26blue				
63.18	[O I]$^3P_1 - ^3P_2$	63.18	45	3
108.07	o-H_2O 2_{21}-1_{10}		$<$2.7	
113.54	o-H_2O 4_{14}-3_{03}	113.61	5	1
124.19	CO 21-20		$<$2.8	
130.37	CO 20-19	130.26	2.2	0.6
137.20	CO 19-18	137.07	2.3	0.6
144.78	CO 18-17	144.72	2.4	0.8
145.53	[O I]$^3P_0 - ^3P_1$		$<$2	
153.27	CO 17-16	153.31	3.0	0.8
157.74	[C II]$^3P_{3/2} - ^3P_{1/2}$	157.75	35	1
162.81	CO 16-15	162.77	4.0	0.7
173.63	CO 15-14		$<$5	
HH26IR				
63.18	[O I]$^3P_1 - ^3P_2$	63.20	39	3
137.20	CO 19-18		$<$2	
144.73	CO 18-17	144.90	2.4	0.5
145.53	[O I]$^3P_0 - ^3P_1$		$<$1.5	
153.27	CO 17-16	153.20	2.6	0.6
157.74	[C II]$^3P_{3/2} - ^3P_{1/2}$	157.77	29.0	0.9
162.81	CO 16-15	162.83	3.4	0.7
173.63	CO 15-14		$<$4	
HH26red				
63.18	[O I]$^3P_1 - ^3P_2$	63.22	19	3
145.53	[O I]$^3P_0 - ^3P_1$		$<$1.5	
157.74	[C II]$^3P_{3/2} - ^3P_{1/2}$	157.77	43	1

† $|\lambda_{\rm vac} - \lambda_{\rm obs}|$ slightly exceedes half of the resolution element.

largest number of molecular transitions, with CO transitions from J_{up}=16 to J_{up}=20 and the 4_{14}-3_{03} o-H_2O line at 113.5 μm; towards the infrared source HH26IR the CO lines from J_{up}=16 to J_{up}=18 were detected while at the HH26red position no molecular lines were detected. Fig. 4 shows continuum subtracted spectra towards HH25MMS, HH26blue and HH26IR.

In Table 2 we also report the upper limits of the [O I]145μm lines, the CO lines with J_{up} value adjacent to the detected transitions and, for HH26blue, the upper limit of the 108.1 μm o-H_2O line; these upper limits will be used in the following analysis aimed to derive the physical parameters of the emitting regions.

3.1. Molecular line fitting

In order to estimate the physical conditions in the emitting gas, we solved the equations of the statistical equilibrium for the CO and H_2O molecules by assuming the radiative Large Velocity Gradient (LVG) approximation and a plane-parallel geometry. Our CO and o-H_2O models predict the level populations of the first 60 and 45 pure rotational levels respectively; detailed information on the adopted radiative and collisional rates as well as on the model assumptions are given in Giannini et al. (1999) for the CO model and in Nisini et al. (1999) for the H_2O model. Since the LVG model depends on a large number of free parameters (gas kinetic temperature, density, intrinsic linewidth, column density and filling-factor), and because the flux uncertainties are quite high, the physical conditions of the emitting region cannot be uniquely constrained by the data, but only a range of values can be given. This also means that meaningful fits were possible only for two sources, namely HH25MMS and HH26blue, in which enough lines were detected.

3.1.1. HH25MMS

Since we observed only three o-H_2O transitions on HH25MMS, we first fitted the CO lines and then checked the derived parameters for consistency with the o-H_2O line fluxes, under the assumption that CO and water originate in the same excitation conditions. In particular, the gas temperature and volume density were derived from the shape of the CO line flux distribution plotted as a function of J_{up}, obtaining T=150-550 K and $n_{\rm H_2}$=5 10^5-8 10^6 cm^{-3} (Fig. 5). In the fit we assumed a linewidth of 15 km s^{-1}, which is about the maximum velocity observed in the outflow; with this adopted value the modelled lines have an optical depth slightly less than 1 and can therefore be used to constrain the CO column density which ranges from 9 10^{17} to 6 10^{18} cm^{-2}. Finally, from the absolute flux of the observed lines, we estimate an emitting region size of $\sim$3 arcsec diameter which corresponds, for a distance of 400 pc, to $\sim$0.006 pc.

The three detected o-H_2O transitions are the backbone lines below the 4_{14} energy level; these transitions connect the lowest levels of each ladder specified by the rotational number J (see e.g. the H_2O energy level diagram in Nisini et al. 1999) and have strong radiative coefficients. The o-H_2O line fluxes

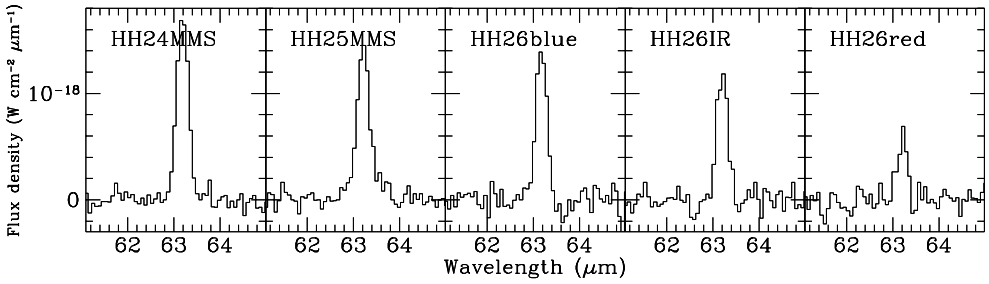

Fig. 3. Continuum subtracted LWS spectra of the [O I]63μm line in the 5 targeted fields.

Table 3. Physical parameters derived by molecular line fitting.

source	T (K)	$n_{\rm H_2}$ (cm^{-3})	$N_{\rm H_2O}$ (cm^{-2})	$N_{\rm CO}$ (cm^{-2})	*diameter* ($''$)	*diameter* (pc)
HH24MMS	650-1400	$5\,10^6$-$5\,10^5$	-	-	-	-
HH25MMS	150-550	$8\,10^6$-$5\,10^5$	$2\,10^{16}$-$9\,10^{15}$	$6\,10^{18}$-$9\,10^{17}$	$\sim$3	~ 0.006
HH26blue	1200-1800	$5\,10^4$-$1\,10^4$	$2\,10^{16}$-$6\,10^{15}$	$2\,10^{17}$-$9\,10^{16}$	5-10	0.01-0.02

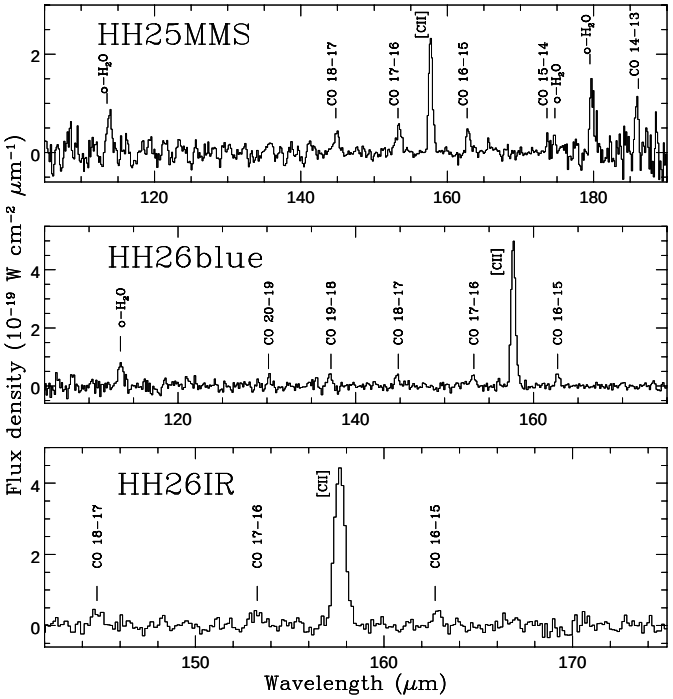

Fig. 4. Continuum subtracted LWS spectra of HH25MMS, HH26blue, HH26IR in the wavelength range in which molecular lines have been detected.

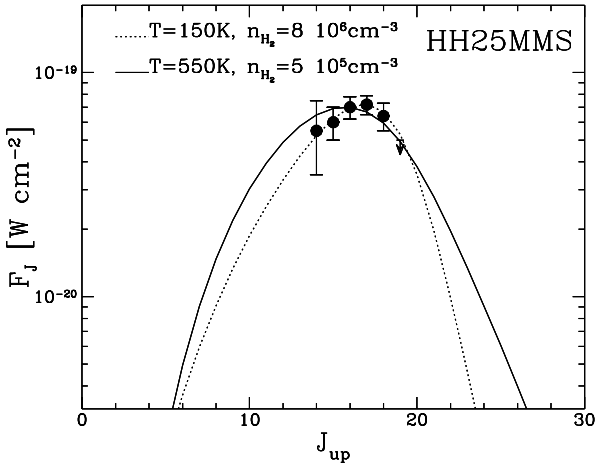

Fig. 5. The observed CO line fluxes in HH25MMS (filled dots) and LVG model fits. The solid and dotted lines are, respectively, for the warmest and coldest model fitting the data.

are consistent with the ranges of temperature and density estimated from the CO fits; however, the lowest temperature fit gives a better match to both the absolute water line fluxes and the emitting size as derived from the CO fit. The H_2O column density is $\sim 10^{16}$ cm^{-2}, which, compared with the derived CO column density and assuming X(CO)=10^{-4}([1]), corresponds to an H_2O abundance in the range $3\,10^{-7}$-10^{-6}.

[1] Gibb & Little (1998) have found that CO may be highly depleted (by more than a factor of 10) towards all the HH24–26 cores. The ISO observations however trace warm regions, where all the CO originally depleted onto grains has probably already returned to the gas-phase due to the elevated temperatures.

The derived temperature is significantly low compared with the temperatures typically traced by the H_2 2.12 μm line ($T \sim$ 2000 K), which is seen to be associated with a collimated string of knots emanating from the Class 0 source (25A, 25B, 25C and 25D in Fig. 1). This indicates that strong temperature gradients may be present in the region. We calculated that the molecular luminosity is ~ 0.033 L$_\odot$ for CO and 0.023 L$_\odot$ for H_2O, while the luminosity emitted in ro-vibrational H_2 lines is estimated to be 0.03 L$_\odot$. The H_2 luminosity is calculated as 10 times the luminosity of the (1-0)S(1) line taken from Davis et al. (1997); the factor 10 is the ratio between the total H_2 and the (1-0)S(1) line luminosities for a gas at 2000 K in LTE conditions. Comparing these values with the luminosity due to [O I]63μm (0.024 L$_\odot$) we conclude that radiative cooling in the region is mainly achieved through re-emission from the molecular transitions: in particular the "warm" (CO+H_2O) gas component seems to dominate the "hot" (H_2) gas. The latter could however be highly understimated if a significant amount of extinction is present in the region.

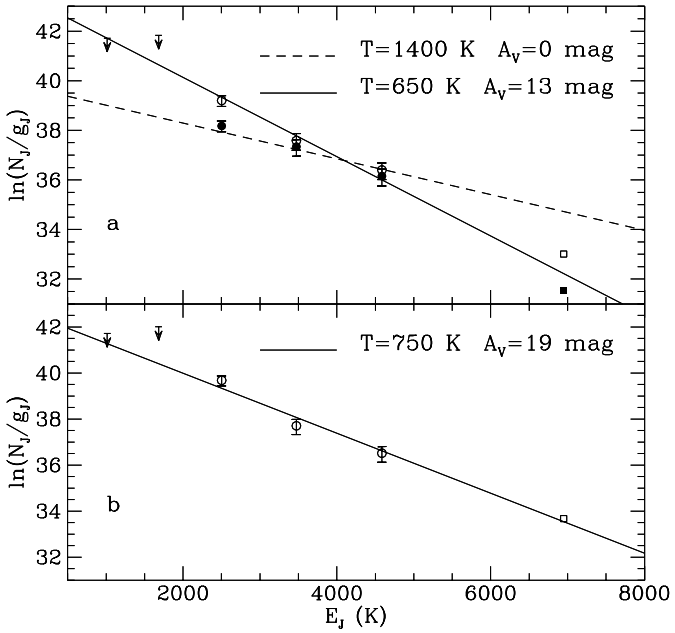

Fig. 6a and b. Rotational diagram for the pure rotational H_2 lines observed with SWS (circles) and the (1-0)S(1) ro-vibrational line (squares) for HH24MMS. In panel **a** we show the fits obtained considering only the SWS lines corrected by A_V=13 mag (open circles) and A_V=0 mag (filled circles), corresponding to a temperature of T=650 K (solid line) and 1400 K (dashed line) respectively. Panel **b** shows the best fit obtained including also the (1-0)S(1) line for A_V=19 mag and T=750 K.

3.1.2. HH24MMS

The observed pure rotational H_2 lines, being optically thin and thermalised, can be effectively used to estimate the gas temperature by means of a rotational diagram. A linear relationship exists, under LTE conditions, between the natural logarithm of the column density of the upper level of each transition (N_J), divided for the statistical weight (g_J), and the energy of the level (E_J): $\ln(N_J/g_J) \propto -E_J/T$; the slope of this straight line is the reciprocal of the excitation temperature. The rotational diagram can also be used to give a rough estimate of the extinction by considering that the S(3) line at 9.7 μm is more sensitive to extinction corrections, lying in the middle of the silicate absorption feature. By imposing that the S(3) transition should lie on the same straightline derived from the S(4) and S(5) transitions and taking into account the associated errors (see Fig. 6a), we derive a gas temperature ranging from 650 to 1400 K and a maximum value for the visual extiction of 13 mag adopting the Rieke & Lebfofsky (1985) extinction law. This value is affected by a relative error of a factor $\sim$2 due to the uncertainty on the $A_{9.7\,\mu m}$ value (Draine 1989).

The SWS beam centered on the Class 0 source also includes the compact H_2 jet (Bontemps et al. 1996) traced by the 2.12 μm line. Although this line, coming from a vibrational transition at much higher excitation energy, is not necessarily associated with the pure-rotational transitions observed by SWS, it is however possible to check if all of these lines could originate from the same gas component at a single temperature. In Fig. 6b we show the best fit we obtain, including the 2.12 μm line, and assuming as emitting region size the 2.12 μm emission size ($\sim 10^{-9}$ sr). While the fitted temperature, T=750 K, is still in the range that we obtained fitting only the (0-0) lines, a larger extinction (A_V=19 mag) is needed to increase the observed 2.12 μm flux to a value compatible with the other lines.

In the LWS spectrum we have detected only one CO line at J_{up}=17 and we assumed that this is the most luminous CO transition, as supported from the fact that the adjacent lines have lower flux upper limits. If the observed CO and H_2 come from the same excited gas, the range of temperatures (650-1400 K) derived from the H_2 analysis can be used to estimate the gas density, which turns out to lie between $5\,10^5$ and $5\,10^6$ cm^{-3}. These values are similar to those estimated in HH25MMS, as expected since both sources are associated to environments with densities in excess of $\sim 10^6$ cm^{-3} (Gibb & Heaton 1993). However, the high J CO line could also be emitted by the shocked gas in 24A (see Fig. 1) which is not encompassed by the SWS beam. In this case we are not allowed to assume the temperature derived from the (0–0) H_2 lines and the observed CO line could also originate from gas colder than 500 K (but warmer than $\sim$200 K) with a density larger than 10^7 cm^{-3}.

The total H_2 luminosity contained in the SWS aperture gets a similar contribution from the observed NIR ro-vibrational lines (L_{NIR}=0.0018 $L_\odot$, determined as ten times the 2.12 μm flux in Bontemps et al. 1996) and the (0-0) lines (0.003 $L_\odot$). However, correcting the NIR emission by an extinction of 19 mag, the L_{NIR} (0.015 $L_\odot$) exceeds the SWS contribution by a factor of 5. If we consider the larger LWS beam, a considerable contribution to the H_2 cooling also comes from the 24A knot (L_{NIR}=0.0095 $L_\odot$, Davis et al. 1997); in this case a lower limit of the total H_2 luminosity of 0.028 $L_\odot$ can be estimated; this value is of the same order of the CO and the [O I]63μm luminosity (0.02 $L_\odot$ and 0.027 $L_\odot$ respectively).

3.1.3. HH26IR and its outflow

In the blue lobe of the outflow (HH26blue), the flux of the CO lines decreases with increasing rotational quantum number J_{up}, which implies that we have not observed the peak of the CO flux distribution (see Fig. 7). This, together with the flux errors, permits only a rough estimate of the gas temperature and density. The average density in the region contained in the LWS beam is $\sim 10^4$ cm^{-3} (Gibb & Heaton 1993) and, while a density enhancement on small scales due to shock compression or clumpy structures might be expected, it is very unlikely that the local density of the shocked gas is less than the average for the cloud. When fitting the CO lines we have therefore not considered volume densities less than 10^4 cm^{-3}. The derived parameter ranges are T= 400–1800 K and n_{H_2}=1 10^4 -2 10^6 cm^{-3} (Fig. 7). For these cases the modelled lines are optically thin, so that the predicted fluxes are independent of the adopted gas velocity and cannot be used to constrain the CO column density. However, a first order estimate of the column density and filling factor can be deduced from both the absolute fluxes and the gas density, by assuming a CO abundance with respect to H_2 of 10^{-4} and that

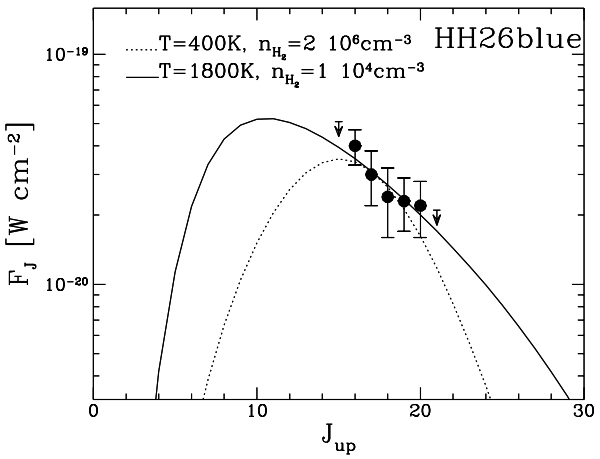

Fig. 7. The same as Fig. 5 for HH26blue.

the width and depth of the emitting region are similar (Giannini et al. 1999).

Although we have detected only one H_2O line, namely the 4_{14}-3_{03} transition at 113.5 μm, the upper limit to the 2_{21}-1_{10} at 108.1 μm, covered by the same LWS detector, can be used to constrain the excitation conditions. In Fig. 8 the expected ratio of the 108.1μm/113.5μm water lines is shown as a function of density and temperature. The two plots also show how this ratio depends on $N_{\rm H_2O}/\Delta v$, the water column density divided by the linewidth. For high values of the water column density ($N_{\rm H_2O}/\Delta v$=10^{15} cm^{-2} km^{-1} s), only low gas densities ($n_{\rm H_2} \lesssim 5\ 10^4$ cm^{-3}) are consistent with the upper limit of the 108.1μm/113.5μm ratio and, to be also consistent with the CO fitting results, higher temperature (T>1200 K) models have to be assumed; also for lower water column densities ($N_{\rm H_2O}/\Delta v$=10^{11} cm^{-2} km^{-1} s) similar values have been derived.

In conclusion, to simultaneously fit both the CO and H_2O emission, temperature and density ranges of T=1200–1800 K and $n_{\rm H_2}$=(1-5)10^4 cm^{-3} have been derived. With these values we obtain $N_{\rm CO}$=(9-20)10^{16} cm^{-2} and $N_{\rm H_2O}$= (6-20)10^{15} cm^{-2} and an emitting area ranging between 5 and 10 arcsec in diameter (corresponding to 0.01–0.02 pc).

The cooling due to CO and H_2O ($\sim$0.05 L$_\odot$) exceeds the contribution due to the [O I]63μm (0.022 L$_\odot$) and is slightly less than the H_2 luminosity (estimated to be $\sim$0.062 L$_\odot$, Davis et al. 1997); therefore the molecular lines are the main channel through which the energy is radiated away. The cooling contributions of the various species relative to the total gas cooling will be analysed in the next section within the framework of different excitation models.

The three CO lines detected towards HH26IR, are unable to significantly constrain alone the local physical parameters. However, they do show similar line ratios to the HH26blue lines and since in the red lobe we do not detect any CO line, it is reasonable to assume that this CO emission is associated to the blue outflow lobe. We have therefore checked that the CO lines detected in the HH26IR measurement are fitted by the same physical parameters derived in the blue lobe, *i.e.* $n_{\rm H_2}$=10^4 cm^{-3},

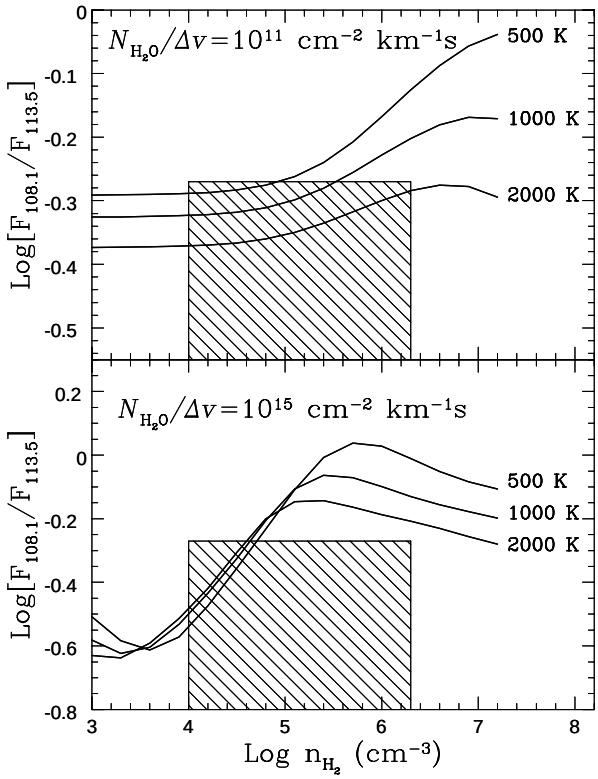

Fig. 8. 108.1 μm/113.5 μm water line ratios *vs* gas density predicted by the LVG model for three temperatures (500, 1000, 2000 K) and for two values of $N_{\rm H_2O}/\Delta v$. The dashed region is limited by the density range derived from CO line fitting and the upper limit ratio obtained on HH26blue by using the upper limit flux of the 108.1 μm.

T=1800 K. The derived emitting size of $\sim$100 arcsec^2, is remarkably similar to the size of the 26A knot (about 95 arcsec^2, see Fig. 1) suggesting that the bulk of the observed emission can originate from this knot.

4. Spectral energy distributions

The emission line spectra discussed so far lie over a dust continuum spectrum which is an important piece of information for an evaluation of the spectral energy distribution (SED) of the various sources. This is especially true for the Class 0 sources, whose SED is expected to peak at wavelengths longer than 100 μm. In Fig. 9 the flux densities obtained from our spectra are combined with other observations available in literature to construct the SEDs of the three sources HH24MMS, HH25MMS and HH26IR in the wavelength range of 50 - 1300 μm. The ISO-LWS data (open circles) are obtained by averaging the fluxes in each detector and the associated error corresponds to the 30% flux calibration uncertainty. Other measurements plotted are IRAS and JCMT (Ward-Thompson et al. 1995; Gibb & Davis 1998), KAO (Cohen et al. 1984), CSO and IRAM (Lis et al. 1999) data. If we look at the ISO fluxes, we note that for the three sources there is an apparent change in the SED slope for wavelengths longer than 100 μm. A likely explanation of this behaviour is the contamination by the strong background cloud

emission which, in the large LWS beam, gives a not negligible contribution at longer wavelengths (see for example the 350 μm map by Lis et al. 1999). This background emission could be in principle removed by subtracting the emission from HH26red, which is the only off-source pointing in the region (see Fig. 1). However diffraction effects from HH26IR at the edge of the beam, make this pointing not useful for this purpose. Source confusion is also present to different extent in all the three objects. In HH25MMS our measurements at 60 and 100 μm are consistent with the IRAS data, while KAO fluxes, obtained with a smaller beam, are significantly below both these values, indicating the presence of diffuse, large scale emission. SSV59 strongly contaminates the spectrum of HH26IR, being just at the edge of the LWS field of view. Finally, the beam centered on HH24MMS encompasses the IR source SSV63, which is associated with a relatively bright IRAS source and has a strong emission at 350 μm (Lis et al. 1999).

The above discussion highlights the difficulties to use the measured SEDs for any comparison with detailed dust emission models. However, a rough estimate of the sources color temperature made between 150 and 350 μm assuming a dust emission coefficient β = 1.5, leads to values of $\sim$ 25 K for HH24MMS and HH25MMS and $\sim$ 40 K for HH26IR, as expected given the apparently more evolved phase of this latter source.

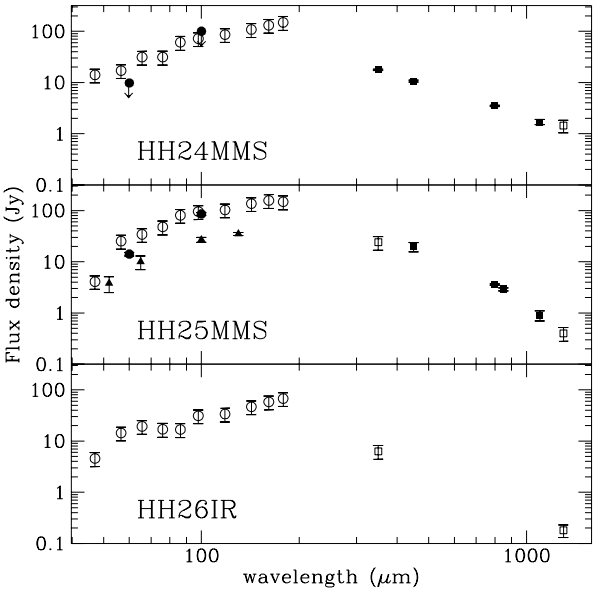

Fig. 9. Observed spectral energy distributions of the three sources: HH24MMS (top), HH25MMS (middle) and HH26IR (bottom). Open circles are obtained from the ISO-LWS observations by averaging the flux densities in each detector. The other symbols are IRAS (filled circles), KAO (filled triangles, Cohen et al. 1984) and ground based observations (filled squares from Ward-Thompson et al. 1995 and Gibb & Davis 1998 and open squares from Lis et al. 1999).

5. Discussion

5.1. Shock excitation

The investigated region shows the presence of a strong shock activity associated with the outflowing gas; it is thus very likely that most of the observed emission is excited in such shocks. We will therefore analyse the consistency of our observations with current shock models.

Among the three observed positions, the HH26blue position shows the richest far infrared spectrum. From Fig. 1 and Table 2, we note in particular that both the molecular and the [O I] emission seem to be correlated with the H_2 2.12 μm intensity along the outflow. This suggests that the shock excitation in the red lobe is less energetic than in the blue one and that the lower H_2 luminosity in this part of the flow cannot simply be a consequence of a larger reddening. An explanation for this difference in the flow excitation may be given considering the density structure of the cloud material into which the flow is expanding (see for example the HCO^+ maps by Gibb & Heaton 1993 and Gibb & Little 1998). The blueshifted gas appears to be flowing into a high-density cloud environment and thus the stellar jet would be expected to experience strong shock interactions as it strikes against the molecular clumps labelled E and F by Gibb & Heaton (1993). On the contrary the red counterpart appears to be in a region of lower and more uniform density, allowing the gas to flow more freely.

Schwartz et al. (1987) observed several near infrared H_2 rovibrational lines from the HH26A knot, and from their absolute intensities and intensity ratios derived an excitation temperature of about 2100 K. This value is very similar to the temperature derived from the far infrared molecular lines ($\sim$ 1800 K), suggesting that the various molecular species (H_2, H_2O and high-J CO) are excited in similar conditions. The total luminosity radiated from the blue lobe of the flow by both the atomic and molecular lines is comparable to the outflow kinetic luminosity ($L_{\rm kin}$=0.16 $L_\odot$, Gibb & Heaton 1993), which indicates that the observed emission lines are excited from the shock generated by the impact of the stellar wind with the molecular cloud.

The two sources HH25MMS and HH24MMS show a higher density of excited gas with respect to HH26IR ($\sim 10^6 {\rm cm}^{-3}$ vs $\sim 10^4$ cm^{-3}). This is somehow expected since they are both Class 0 objects with a significant amount of material in their environment; dense shocks are therefore more likely to develop along their outflows. These two Class 0 sources show indeed a similar nature. They both have VLA counterparts (Bontemps et al. 1995) and in addition, they are both associated with HCO^+ and CS molecular clumps whose central densities are higher than 10^6 cm^{-3}. Moreover, they both seem to drive compact jet-like flows: in HH25MMS the outflow has been traced by means of CO 3-2 emission (Gibb & Davis 1998) and in HH24MMS jet-like H_2 2.12 μm and radio emission is seen (Bontemps et al. 1996) ([2]).

Despite these similarities, they however exhibit some differences in their FIR spectra, as can be seen in Table 4 in which

[2] HH24 contains at least two strong collimated optical jets (Mundt et al. 1991), however they are not associated with the MM source but appear originated from the IR source SSV63. Of the shocked optical knots, only HH24A is also associated with H_2 2.12 μm emission (Davis et al. 1997); this knot is thought to represent the point of interaction between the C-E jet from SSV63 and the compact flow from the MM source.

Table 4. Cooling from the [O I]63 μm, CO, H_2O and H_2 (calculated as 10 times the 2.12 μm line luminosity taken from Davis et al. 1997) for the observed objects (column 2, 3, 4 and 5 respectively). All the values are expressed in $L_\odot$ units.

source	$L_{[\mathrm{O\,I}]63\,\mu\mathrm{m}}$	L_{CO}	$L_{\mathrm{H_2O}}$	$L_{\mathrm{H_2}}$
HH24MMS	0.027	0.020	-	0.028†
HH25MMS	0.024	0.030–0.037	0.020–0.026	0.030
HH26blue	0.022	0.027–0.033	0.020	0.062
HH26IR	0.019	-	-	0.046
HH26red	0.0094	-	-	0.009

† the luminosity of the 24B knots is corrected by an extinction of 19 mag and the contribution of the H_2 lines observed with SWS is also included.

the relative cooling due to the different species are given. As already noticed, in HH25MMS the gas cooling is dominated by molecular emission. The ratio of the [O I]63μm luminosity to the luminosity in CO, H_2 and H_2O for this source is $\sim$0.3; at the derived temperature range (T=150–550 K), a significant contribution is also expected from the pure rotational H_2 transitions which is not taken into account here. On the contrary, less FIR emission is observed in the form of molecular transitions in HH24MMS, where the ratio of [O I]63μm over molecular luminosity is 0.8 (0.6 if the extinction is taken into account). The characteristics of the shock activity in the surroundings of these sources appears to be different also in the NIR. The well localised H_2 2.12 μm emission associated with the HH24MMS source is weaker than in the HH25 and 26 knots, which led Bontemps et al. (1996) to invoke a large extinction in the region. We have shown however that the visual extinction, averaged across the SWS beam, is $\leq$19 mag ($\lesssim$30 mag if we take into account the uncertainty on the extinction curve) and not the 50–100 mag derived by Bontemps et al. (1996) from the millimeter continuum, assuming a spherical protostellar envelope; this suggests that the jet may have already opened a cavity in the envelope.

In any case, the prevalence of molecular cooling over the [O I]63μm emission in the three sources, together with the relatively high temperatures derived at least for HH26blue and HH24MMS, are both evidences which point to excitation by a slow non-dissociative *C*-shock more than to a *J*-type shock (Draine et al. 1983; Hollenbach & McKee 1989; see also Nisini et al. 1999 for a comparison of the predictions by the different shock models). Temperatures in the range 500–2000 K are indicative of shock velocities $\sim$15–25 km s^{-1} (Kaufman & Neufeld 1996): in such a shocks the cooling due to H_2 ro-vibrational lines increases with the temperature, as we observe in HH26blue which shows the largest value of L_{H_2} (see Table 4). However the contribution of the water cooling is much lower than predicted given the fact that at $T > 400$ K all of the oxygen not locked into CO would be expected to be converted into water. This result is not totally surprising; indeed the water abundance and its relative cooling have already been found to be lower than predicted by models (i.e. Kaufman & Neufeld 1996) in the majority of the outflows that have been observed by ISO (Saraceno et al. 1999). The only exception is the Class 0 source L1448-mm, where despite conditions similar to HH26blue ($T \sim$1400 K and $n_{\mathrm{H_2}} \sim 6\,10^4$ cm^{-3}), the water abundance is $\sim 5\,10^{-4}$, i.e. more than one order of magnitude higher than here (Nisini et al. 1999). Possible explanations for this may be either that less atomic oxygen is available to be incorporated into water due to depletion onto the grains, or that part of the water could rapidly be depleted onto cold grains once the shock is passed, as suggested by some time dependent models (Bergin et al. 1998). We stress however that the estimated water abundance is still significantly greater than expected in quiescent clouds (which is predicted to be about 10^{-8}-10^{-7}). That in the considered regions there is a significant chemical reprocessing due to the shock passage is also testified for HH25MMS, where Gibb & Davis (1998) observed a significant abundance enhancement for slow shock tracer species such as SiO and methanol.

While the observed molecular emission can be better accounted for in the framework of *C*-shock models, we cannot however overlook the few but strong evidences in favour of the presence of a *J*-shock in the region; firstly, the presence of the optical HH objects, which testifies to the high excitation and ionization and secondly the high radial velocity of these Herbig Haro ($\gtrsim$100 km s^{-1}) (Jones et al. 1987). An additional test for the presence of a strong component due to a *J*-shock can be made by using the [O I]63μm emission; it has been indeed realised by Hollenbach (1985) that the [O I]63μm line luminosity is proportional to the rate of mass lost from the star providing that it directly traces the dissociative shock due to the impact of the high velocity star wind on the ambient medium. Alternatively, the wind mass loss rate may be also estimated from the spatial maps of mm CO lines, in the hypothesis of momentum conservation and assuming a wind velocity. For HH26IR we consider the flow parameters derived from the CO observation by Gibb & Heaton (1993) and assume a wind velocity equal to the radial velocity of HH26 (i.e. $\sim$130 km s^{-1}, Jones et al. 1987) obtaining a mass loss rate of $1.8\,10^{-6}$ M$_\odot$ yr^{-1} in the blue lobe of the outflow. From the [O I]63μm luminosity, we derive a mass loss rate of $(2.1\pm0.1)\,10^{-6}$ M$_\odot$ yr^{-1}, which is similar to the value given from the mm observations; this indicates the validity of the underlying hypothesis that the [O I] emission is mainly due to a dissociative shock and that it provides the dominant cooling process. This result is in broad agreement with the general trend found between these two mass loss determinations in a sample of HH objects observed by LWS (Liseau et al. 1997).

On the other hand, from the HH25MMS flow parameters given by Gibb & Davis (1998) a mass loss rate equal to $1.3\,10^{-7}$ M$_\odot$ yr^{-1} is derived (allowing for a factor of two due to the incomplete mapping of the flow), while the [O I]63μm luminosity gives $(2.3\pm0.1)\,10^{-6}$ M$_\odot$ yr^{-1} which is more than a factor ten larger. One possible reason for this discrepancy is that the Gibb and Davis flow parameters are not corrected for the outflow inclination which is likely to be significant given the orientation close to the plane of the sky of this flow. This seems in fact the most plausible explanation af-

ter having considered additional sources for the [O I] excitation. The *C*-shock component alone cannot account for an excess of [O I] emission. Excitation by photodissociation will be considered in the next paragraph where we show that its contribution can account for at maximum 30% of the total [O I] luminosity in HH25MMS. The possibility that a significant fraction of [O I] is emitted directly in a protostellar disk accretion shock can also be investigated. According to the Neufeld & Hollenbach (1994) model, the [O I]63μm luminosity in such high density shocks cannot exceed $\sim 10^{-4}$ $L_\odot$ unless very large accretion rates (larger than 10^{-4} $M_\odot$ yr^{-1}) are considered. [O I]63μm can also arise from the protostar collapsing envelope (Ceccarelli et al. 1996); however, its luminosity is never expected to be more than one tenth of the value observed in HH25MMS.

In HH24MMS the mass loss rate derived from [O I]63μm luminosity is $(2.6\pm0.1)\,10^{-6}$ $M_\odot$ yr^{-1}; this value cannot be however compared with any CO map determination since no millimeter data are available for this flow.

In conclusion, the different observational evidence gathered for the three investigated sources cannot be explained by a single shock component: a mixture of *C*- and *J*-shocks seem to best reproduce the cooling due to the different species as well as the various velocity components. This could for example be achieved by considering a curved shock (bow shock); in this case the maximum shock velocity is achieved at the head of the bow thus producing a dissociative shock, while in the tail the velocity at which the jet strikes the ambient medium is reduced and an oblique *C*-shock can be produced (Smith 1991). The evidence that HH24MMS lacks a molecular cooling as strong as for the other two sources can be explained by two different pictures: 1) the jet emanating from the MM source produces a strong dissociative shock emitting primarily in the [O I]63μm line and at cm wavelengths; only a small part of the energy is released in the form of H_2 emission which could originate from either the H_2 reformation plateau as predicted for *J*-type shocks (Hollenbach & McKee 1989) or from a different and weaker shock in the bow tails of the jet; 2) the observed [O I] emission comes mainly from the optical HH knots that are not associated with the MM source, while the jet from HH24MMS is energetically too weak to produce strong shock interactions observable by LWS.

5.2. Spatial distribution of [O I] and [C II] and PDR excitation

Inspection of Fig. 1 shows that the region covered by our measurements also includes, in addition to the different shocked knots traced by the 2.12 μm emission, the young objects SSV60 inside the HH26blue pointing, and SSV63 and SSV59 on the edge of the beam centered on HH24MMS and HH26IR respectively. These objects are embedded pre-main sequence stars which are probably not associated with the surrounding shock activity. Despite their relatively low luminosities ($\sim$20 $L_\odot$) the associated FUV flux ($6< E <13.6$ eV) could produce compact photodissociation regions (PDR) able to excite the circumstellar gas (as modelled e.g. by Spaans et al. 1994), so it could be argued

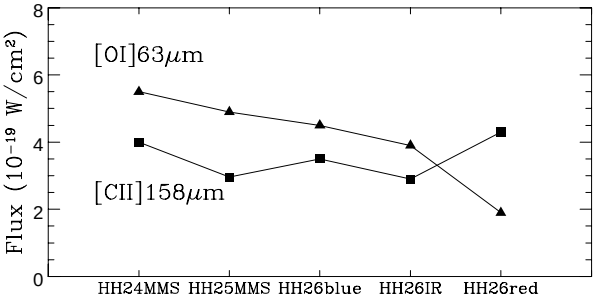

Fig. 10. Line fluxes of [OI]63 μm and [CII]158 μm measured in the observed positions.

that a significant fraction of the [O I]63μm emission results from this contribution in addition to the shock excitation. In principle, the presence of a localised PDR is easily recognisable with an enhancement of the [C II]158μm emission which is dependent on the presence of a FUV field. However, the [C II]158μm flux at the different observed positions is quite uniform (Fig. 10) and in general there is no correlation between this emission and the presence of IR sources in the beams. Therefore we conclude that the FUV fields from these stars provide only a minor contribution to the gas excitation.

On the other hand, this uniformity of the [C II]158μm flux is an indication that the emission arises from the PDR of the ambient molecular cloud exposed to the averaged Galactic field. This in principle could itself be also responsible for part of the [O I]63μm emission. To check for this possibility, we use the PDR model results by Kaufman et al. (1999). According to this model, if we assume a cloud mean density of 10^4 cm^{-3} or less, the observed average [C II]158μm intensity of $2.7\,10^{-5}$ erg s^{-1} cm^{-2} sr^{-1} corresponds to a FUV field of about 3–6 G_0 (where G_0 is the FUV flux expressed in units of the local interstellar value, i.e. $1.6\,10^{-3}$ erg s^{-1} cm^{-2}). With such a field the expected [O I]63μm/[C II]158μm intensity ratio can be 0.5 at maximuum. Looking at Fig. 10, where the flux density of these two lines is plotted versus the different investigated positions, we see that in fact the observed [O I]63μm always exceeds the contribution of the [C II]158μm with the exception of the HH26red position, where a ratio of about 0.5 is reached. Among the targetted positions this is indeed the one where the shock excitation is the faintest and thus where the diffuse PDR should give the largest contribution. We therefore conclude that the diffuse PDR from the ambient cloud may be responsible for most of the [O I]63μm emission only towards HH26red, while in the other positions it can account for a maximum of 40% of the observed flux at worst.

The [O I]145μm line was not detected in any of the LWS spectra. Comparing the upper limit for this line with the detected [O I]63μm line flux, we obtain a lower limit on the ratio [O I]63μm/[O I]145μm ranging from 13 to 26 with an average value of 20. The ratio of this two lines is in principle very sensitive to the hydrogen gas density, irrespective of the excitation mechanism, as soon as the temperature exceeds a value of about 300 K: the derived lower limits indicate in particular densities larger than 10^4 cm^{-3} and are therefore consistent with the values

derived from the analysis of the molecular emission. Although not very stringent, the measured lower limits on this ratio appear to be within the range of expected values. This is not always found in the surroundings of deeply embedded young stellar sources, where values of the [O I]63μm/[O I]145μm ratio much lower than predicted by any physical model have been found. These anomalous ratios have been interpreted as being due to strong absorption of the [O I]63μm line by large columns of cold gas along the line of sight (Saraceno et al. 1998), a situation which does not seem to be present in the HH24–26 region.

6. Conclusions

The analysis of the ISO spectroscopic data obtained in different positions along the HH24–25 and 26 region, shows that the far infrared spectra are dominated by atomic ([O I]63μm line) and molecular (CO and H_2O) transitions excited in shocks. The emission does not appear uniformely distributed but it is strongly correlated with other shock tracers like the H_2 (1-0)S(1) line at 2.12 μm. At variance with this trend, [C II]158μm emission is observed at all the positions and its intensity is not correlated with the presence of the infrared sources in the investigated fields, excluding the occurrence of PDR excitation related to the IR sources.

The shocked regions around HH25MMS and HH24MMS appear to be denser ($n_{\rm H_2}$ $\sim$10^6 cm^{-3}) than along the blue outflow lobe of HH26IR ($n_{\rm H_2}$ $\sim$10^4 cm^{-3}). The derived temperatures are of the order of 150–500 K in HH25MMS, slightly higher in HH24MMS (T $\sim$ 650–1400 K) and reach values as high as 1800 K in the blue lobe of the HH26IR flow. Such a difference in temperature is probably related with the different shock velocities in the three regions.

Emission from water lines is confined to the positions centered on HH25MMS and in the blue lobe of the HH26IR flow. The estimated water abundances are less than $9\,10^{-6}$, confirming previous findings that the observed water abundance in shock excited regions is generally less than predicted by models.

A mixture of both *C*- and *J*-type shocks is needed to account for all the different components present in the region and to explain the observed FIR emission. We note in particular that the relative strength of these two types of shocks is different among the various positions. In HH25MMS the line cooling is dominated by molecular emission from CO, H_2O and H_2, indicating that the non-dissociative shock is by far the main excitation mechanism. On HH24MMS, at variance, little molecular emission is observed, pointing to a prevalence of a *J*-type shock. Finally, along the HH26IR flow there is a strong component of molecular emission but at the same time the correlation of the [O I]63 μm luminosity with the outflow mass loss rate indicates also the presence of dissociative *J*-shocks.

We finally remark that the total cooling due to the gas components traced by the far infrared lines is always of the same order of magnitude or larger (up to a factor of three in HH25MMS) than the cooling due to H_2 alone, which is usually derived from ground based observations of the 2.12 μm line. This finding needs to be taken into account in future analyses of the energy balance along the outflows.

References

Andrè P., Ward-Thompson D., Barsony M., 2000, *Protostars and Planets IV*, ed. V. Mannings, A.P. Boss & S. S. Russell, University of Arizona Press, in press

Anthony-Twarog B.J., 1982, AJ 87, 1213

Bergin E.A., Melnick G.J., Neufeld D.A., 1998, ApJ 499, 777

Bontemps S., Andrè P., Ward-Thompson D., 1995, A&A 297, 98.

Bontemps S., Ward-Thompson D., Andrè P., 1996, A&A 314, 477

Chini R., Krügel E., Haslam C.G.T., et al., 1993, A&A 272, L5

Cohen M., Harvey P.M., Schwartz R.D., Wilking B.A., 1984, ApJ 278, 671

Clegg P.E., Ade P.A.R., Armand C., et al., 1996, A&A 315, L38

Ceccarelli C., Hollenbach D.J., Tielens A.G.G.M., 1996, ApJ 471, 400

Davis C.J., Ray T.P., Eislöffel J., Corcoran D., 1997, A&A 324, 263.

de Graau, T., Haser L.N., Beintema D.A., et al., 1996, A&A 315, L49

Draine B.T., Roberge W.G. and Dalgarno A., 1983, ApJ 264, 485

Draine B.T., 1989, ESA *Infrared Spectroscopy in Astronomy*, p. 93

Giannini T., Lorenzetti D., Tommasi E., et al., 1999, A&A 346, 617

Gibb A.G., Davis C.J., 1998, MNRAS 298, 644

Gibb A.G., Heaton B.D., 1993, A&A 276, 511

Gibb A.G., Little L.T., 1998, MNRAS 295, 299

Hollenbach D.J., 1985 Icarus 61, 40

Hollenbach D.J., McKee C.F., 1989, ApJ 342, 306

Jones B.F., Cohen M., Wehinger P., Gehren T., 1987, AJ 94, 1260

Kaufman M.J., Neufeld D.A., 1996, ApJ 456, 250

Kaufman M.J., Wolfire M.G., Hollenbach D.J., Luhman M., 1999, ApJ 527, 795

Kessler M.F., Steinz J.A., Anderegg M.E., et al., 1996, A&A 315, L27

Lis D.C., Menten K.M., Zylka R, 1999, ApJ 527, 856L

Liseau R., Giannini T., Nisini B., et al., 1997, IAU Symp. 182, *Herbig Haro flows and the birth of low mass stars*, pag. 111

Mundt R., Ray T.P., Raga A.C., 1991, A&A 252, 740

Neufeld D.A., Hollenbach D.J., 1994, ApJ 428, 170

Nisini B., Benedettini M., Giannini T., et al., 1999, A&A 350, 529

Rieke G.H., Lebofsky M.J., 1985, ApJ 288, 618

Saraceno P., Nisini B., Giannini T., et al., 1998, APS Conference series, 132, *Star Formation with the Infrared Space Observatory*, pag. 233

Saraceno P., Nisini B., Benedettini M., et al., 1999, SP-427 *The Universe as seen by ISO*, pag. 575

Schaeidt S.G., Morris P.W., Salama A., et al., 1996, A&A 315, L55

Schwartz R.D., Cohen M., Williams P.M., 1987, ApJ 322, 403

Smith M.D., 1991, MNRAS 253, 175

Spaans M., Tielens A.G.G.M., van Dishoeck E.F., et al., 1994, ApJ 437, 270

Strom K.M., Strom S.E., Vrba F.J., 1976, AJ 81, 308

Swinyard B.M., Clegg P.E., Ade P.A.R., et al.,1996, A&A 315, L43

Ward-Thompson D., Chini R., Krugel E., Andrè P., Bontemps S., 1995, MNRAS 274, 1219